NEW STRATEGIES INVONVING UPCONVERTING NANOPARTICLES FOR DETERMINING MODERATE TEMPERATURES BY LUMINESCENCE THERMOMETRY

Ol.A. Savchuk,[1] J.J. Carvajal,[1,*] M.C. Pujol,[1] J. Massons,[1] P. Haro-González,[2] O. Martínez,[3] J. Jiménez,[3] M. Aguiló,[1] F. Díaz[1]

[1]*Física i Cristal·lografia de Materials i Nanomaterials (FiCMA-FiCNA) and EMaS, Universitat Rovira i Virgili (URV), c/Marcel·lí Domingo s/n E-43007, Tarragona, Spain*

[2]*Fluorescence Imaging Group, Departamento de Física de Materiales, Facultad de Ciencias, Universidad Autónoma de Madrid, C/Francisco Tomás y Valiente 7, E-28049, Madrid, Spain*

[3] *GdS-Optronlab, Departamento Física Materia Condensada, Univ. de Valladolid, Edificio I+D, Paseo de Belén, 11, 47011, Valladolid, Spain*

*Corresponding author: joanjosep.carvajal@urv.cat

Abstract

Here we analyze alternative luminescence thermometry techniques to FIR, such as intensity ratio luminescence thermometry between the emission arising from two electronic levels that are not necessarily thermally coupled, but that show different evolutions with temperature, and lifetime luminescence nanothermometry in $(Ho,Tm,Yb):KLu(WO_4)_2$ and $(Er,Yb):NaY_2F_5O$ nanoparticles. $(Ho,Tm,Yb):KLu(WO_4)_2$ nanoparticles exhibited a maximum relative sensitivity of 0.61 % K^{-1}, similar to that achievable in Er-doped systems, which are the upconverting systems presenting the highest sensitivity. From another side, $(Er,Yb):NaY_2F_5O$ nanocrystals show great potentiality as thermal sensors at the nanoscale for moderate temperatures due to the incorporation of additional non-radiative relaxation mechanisms that shorten the emission lifetime generated by the oxygen present in the structure when compared to $(Er,Yb):NaYF_4$ nanoparticles exhibiting the highest upconversion efficiency. We used those nanoparticlesfor ex-vivo temperature determination by laser induced heating in chicken breast using lifetime-based thermometry. The results obtained indicate that these techniques might constitute alternatives to FIR with potential applications for the determination of moderate temperatures, with sensitivities comparable to those that can be achieved by FIR or even higher.

1. Introduction

Heat is produced in several processes, which generates an increase of temperature, that in general is interesting to know and be measured. Examples include monitoring the evolution of temperature in chemical reactors [1], detection of "hot spots" in microelectronic devices [2], detection of local temperatures within integrated photonic devices to prevent irreversible damages [3], monitoring heat dissipation during optical trapping [4], monitor temperature changes in microfluidic systems [5] and monitoring metabolic processes in living organisms [6], to name a few.

Typical systems used to control the temperature increment require contact, which generates technological challenges when spatial resolution decreases to the submicron scale. Fortunately, there are various types of non-contact nanothermometry approaches, one of the most attractive of which is luminescence thermometry, based on the temperature-dependent emission intensity, lifetime value, band shape or position of emission bands of luminescent nanoparticles [7,8]. These methods offer relatively high detection sensitivity and spatial resolution in short acquisition time, even in fluids, strong electromagnetic fields and fast moving objects [9-11].

The use of upconversion nanoparticles, which exhibit efficient visible emission properties after excitation in the near infrared, can provide simultaneously the dual function of imaging and temperature sensing at the nanoscale [12].

The potentiality of Er^{3+}, Yb^{3+} codoped upconversion nanoparticles for nanothermometry in the range of moderate temperatures has been especially highlighted [13,14], especially due to the suitable energy gap between the $^2H_{11/2}$ and $^4S_{3/2}$ energy levels of Er^{3+}, which are thermally coupled, using, for instance, $(Er,Yb):NaYF_4$ nanoparticles.

However, there exist other alternative materials and thermometry techniques with potential use for the determination of moderate temperatures that can offer a similar or even higher sensitivity with respect to those offered by Er^{3+}-doped systems. Here, we analyze the possibilitites offered by two dielectric phosphors, $(Ho,Tm,Yb):KLu(WO_4)_2$ and $(Er,Yb):NaY_2F_5O$, by measuring the luminescence thermometry intensity ratio between the emission arising from two electronic levels that are not necessarily thermally coupled, but that show different evolutions with temperature in the former, with sensitivities comparable to those obtained in Er^{3+}-doped systems, and by measuring lifetimes in the second.

2. Experimental section

Synthesis of luminescent nanoparticles. 1.5 at. % Ho, 1 at.% Tm, and 1 at. % Yb doped $KLu(WO_4)_2$ nanocrystals were synthesized by the sol-gel modified Pechini method [20] Analytic grade purity reagents of Ho_2O_3 (99.9999%), Tm_2O_3 (99.9999%), Yb_2O_3 (99.9%), and Lu_2O_3 (99.9999%), were dissolved in hot nitric acid in the specific proportions to form the nitrate precursors. Citric acid (CA) was used as the chelating agent while ethylenglycol (EG) was used as the estherification agent in the synthesis process. The nitrate precursors were dissolved in distilled water with citric acid in a molar ratio of CA to metal cations equal to 1. Ammonium tungstate $(NH_4)_2WO_4$ (99.99%) and potassium carbonate K_2CO_3 (99.99%) were added to the aqueous solution and we heated it at 353 K under magnetic stirring during 24 h until complete dissolution. Further, EG was added to the mixture in a molar ratio [EG]/[CA] = 2. The solution was heated at 373 K in order to evaporate water and generate the polymeric gel. After that, the polymeric gel was calcinated at 573 K for 3 hours, and later at 1023 K for 2 hours to eliminate the organic compounds and crystallize the desired nanoparticles. The raw $(Er,Yb):NaY_2F_5O$ nanoparticles were purchased to Boston Applied Technology.

Raman scattering measurements. Micro-Raman spectra were obtained at room temperature with a Labram HR800 UV Raman spectrometer from Horiba-Jobin-Yvon attached to a metallographic microscope with confocal optics, and equipped with a LN_2-cooled charge-coupled-device (CCD) detector. The excitation was carried out with a UV laser at 325 nm using a 40 X UV microscope objective with 0.5 numerical aperture (NA). The scattered light was also collected by the objective, thus working in a nearly backscattering configuration.

Temperature-dependent luminescent experiments. For upconversion emission measurements, (Ho,Tm,Yb):KLuW nanoparticles were introduced in a Linkam THMS 600 heating stage. The sample was excited with a diode laser emitting at 808 nm, which corresponds to the maximum absorption wavelength of Tm^{3+}. The beam from the laser source was focused on the sample and the emission was collected in $90°$ geometry in order to eliminate the residual laser pump. Emission radiated from the sample was collected and dispersed on a Jobin Yvon HR 460 monochromator. For detection, a Hamamatsu PMTR 928 photomultiplier tube, connected to a Perkin Elmer DSP-7265 lock-in amplifier was used.

Lifetime thermometry. For luminescence decay-time experiments as a function of temperature, (Er,Yb):NaY$_2$F$_5$O nanoparticles were introduced in a Linkam THMS 600 heating stage and excited at 980 nm with an optical parametric oscillator (OPO) from Opotek (Vibrant HE 355 II+UV) with a pulse duration of 6 ns and a repetition frequency of 10 Hz. The fluorescence light emitted by the sample was collected with a microscope objective, transferred to the monochromator for the selection of specific wavelengths, and then detected using a Hamamatsu R928 photomultiplier. The decay of the signal was measured as a function of time with a digital oscilloscope, averaging the signal from 3000 laser pulses.

Lifetime thermal sensing experiments. After calibration, (Er,Yb):NaY$_2$F$_5$O nanoparticles were dispersed in distilled water and injected in a fresh chicken breast. A heating laser with emission at 1090 nm and a pumping laser with emission at 980 nm, spatially overlapping, were simultaneously focused in the chicken breast using a microscope objective. The fluorescence arising from the nanoparticles was collected by the same objective, and after passing the selected filters, was focused into the photomultiplier tube connected to the digital oscilloscope.

3. Results and Discussion

3.1.(Ho,Tm,Yb):KLu(WO$_4$)$_2$ nanoparticles

We studied the upconversion emission of Ho^{3+}, Tm^{3+}, and Yb^{3+} codoped KLu(WO$_4$)$_2$ nanoparticles, and analyzed the possibilities of their emissions for temperature sensing applications. As a host material the KLu(WO$_4$)$_2$ monoclinic matrix has several advantages. For instance, the Yb^{3+} absorption cross-section in KLu(WO$_4$)$_2$ single crystals has been measured to be 11.8×10^{20} cm^2 [15], which is around 15 times bigger than that on Yb^{3+} in YAG crystals [16]. Furthermore, this host allows for large doping concentrations, up to 100%, without emission quenching effects [17]. (Ho,Tm,Yb):KLu(WO$_4$)$_2$ single crystals [18] and nanocrystals [19] have been used, for instance, for the generation of white light through the combination of the blue, green and red light emitted by this material when excited with 980 nm light by tuning the concentrations of the doping ions to equilibrate the intensity of the RGB emissions. Thus, they show a rich emission structure with possibilities to be used in thermal sensing. Its quantum yield in comparison to that reported for (Er,Yb):NaYF$_4$ nanoparticles [20], the most efficient up-converting system presented up to date, is around one order of magnitude lower [21]; however, it is comparable to other up-converting oxide

nanoparticles currently used for nanothermometry applications [22-27]. Furthermore, halide-based materials tend to be hygroscopic, showing relatively poor chemical and photophysical stabilities compared to oxide matrices; on the other hand, most of the preparative routes for halide-based nanoparticles are complex and environmentally harmful.

(Ho,Tm,Yb):KLu(WO$_4$)$_2$ nanoparticles have been synthesized by the sol-gel modified Pechini method. Figure 1 shows a TEM image in which the aspect of these nanoparticles can be seen. Particles show irregular shapes, with sizes below 50 nm, as can be seen in the histogram, in which we statistically analyzed the nanoparticles size distribution, furthermore, a relatively low degree of agglomeration is observed. (Ho,Tm,Yb):KLu(WO$_4$)$_2$ nanoparticles crystallize in the monoclinic system, with spatial group C2/c, as it was reported for single crystals with the same chemical composition [18].
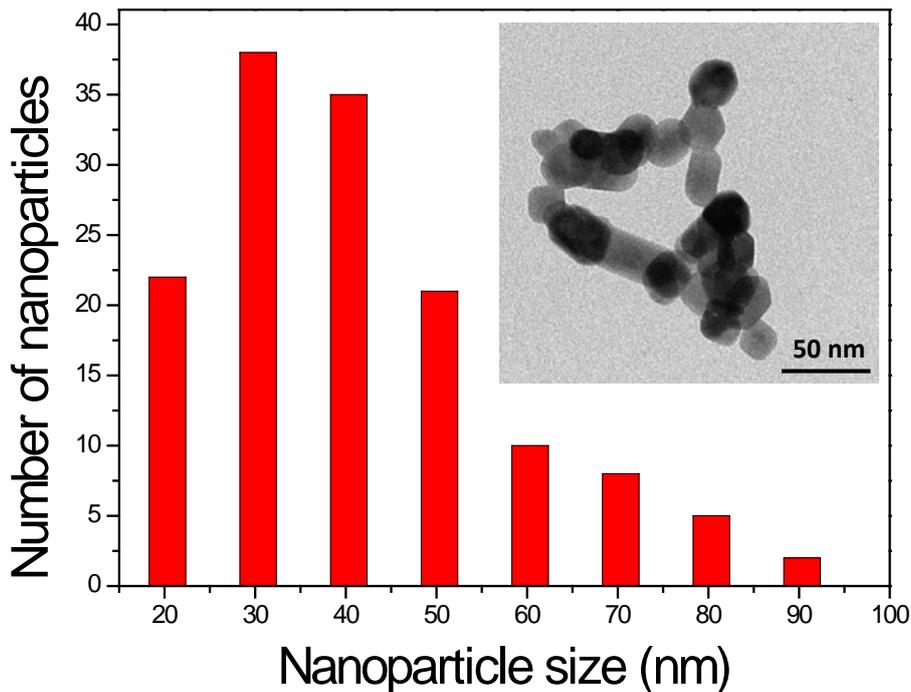
Figure 1. TEM image of (Ho,Tm,Yb):KLu(WO$_4$)$_2$ nanoparticles and histogram showing the mean sizes of these nanoparticles.

Figure 2(a) shows the evolution of the upconversion emission spectra of (Ho,Tm,Yb):KLu(WO$_4$)$_2$ nanocrystals excited at 808 nm in the range of temperatures 22 – 250 ºC, which exhibits three emission bands in the blue, green and red region of the electromagnetic spectrum. In order to understand the origin of the different emission lines, we have studied the upconversion mechanism in detail by pumping at specific

wavelengths in the visible to excite specific energy levels of the different emitting ions. Figure 2(b) summarizes the different excitation and emission mechanisms deduced for this material. From this analysis, it is clear that the green and red emissions arise from different ions of the system, and occurred due to energy transfer processes that are temperature dependent. In fact, we observed that while the green emission generated by Ho^{3+} decreases in intensity when the temperature increased, the red emission intensity generated by Tm^{3+} increased, showing that, despite we cannot consider, strictly speaking, that those levels are thermally coupled, they are somehow thermally linked through phononic processes associated with energy transfer processes. In fact, by increasing the temperature, the multiphonon nonradiative depopulation rate of the $^5S_2$ and $^5F_4$ energy levels of Ho^{3+} (from which the green emission originated) will become faster, populating the $^5F_6$ energy level of this ion. From here, an energy transfer process occurs to the $^3F_2$ and $^3F_3$ energy levels of Tm^{3+} from which the red emission occurs. Thus, although we cannot apply the FIR technique as defined by Wade et al. [28] in that case for temperature sensing purposes, this allows us to apply the intensity ratio technique to analyze the thermal evolution of the emission from these ions, and use these nanoparticles as luminescent nanothermometers.

In order to explore the possibilities of using these nanoparticles as a nanothermometer suitable for moderate temperatures, we have focused on the range of temperature between 22 and 50 ºC. The ratio between the integrated intensities of the two emission bands, located in the red and the green spectral windows, as a function of temperature is plotted in Figure 2(c). The experimental data could be fitted to a linear equation: I_{red}/I_{green} = -0.8 + 0.0061T. The relative sensitivity, calculated as the first derivative of the intensity ratio divided by the intensity ratio is plotted in Figure 2(d). This parameter allows us to compare the performance of our system with respect to other luminescent thermometers reported before. The maximum relative sensitivity was found to be 0.61 % $ºC^{-1}$, similar to those previously reported for Er^{3+} based systems, which up to date were the highest ones reported in the literature [29,30]. Thus, Tm^{3+} and Ho^{3+} ions in the $KLu(WO_4)_2$ host might become a competing technology with Er^{3+} for thermometry applications.
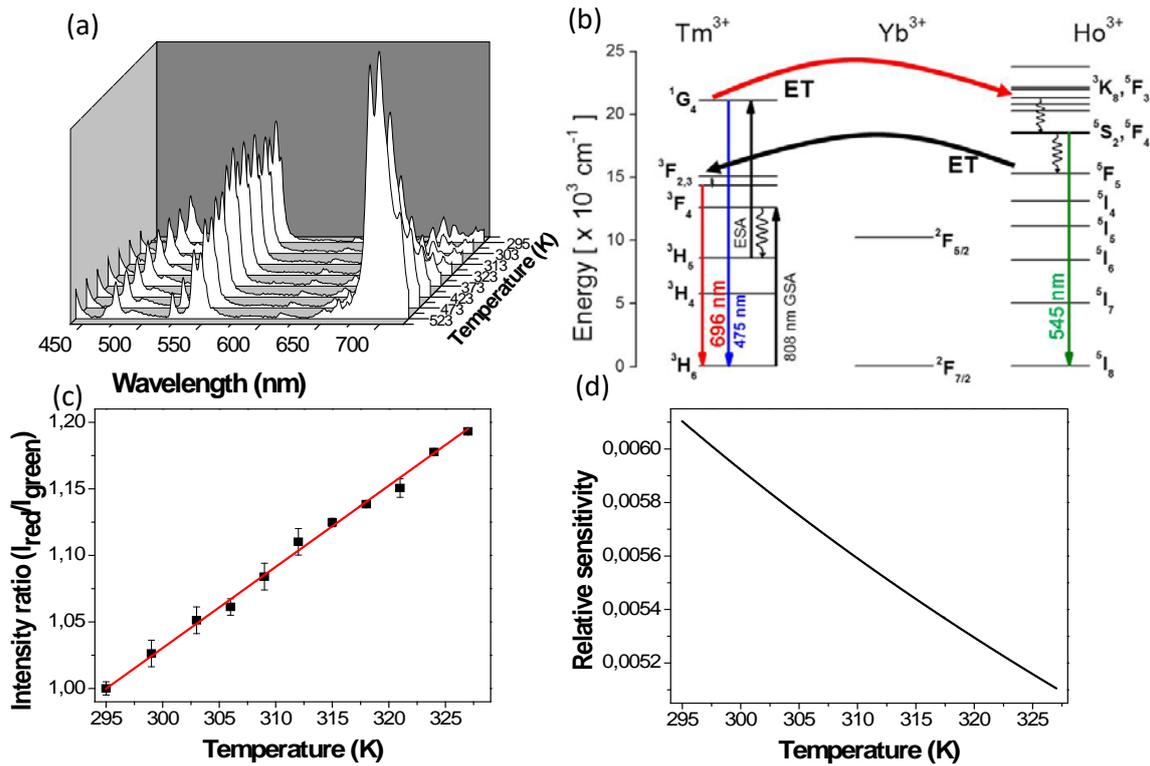
Figure 2. (a) Evolution of the emission spectra of (Ho,Tm,Yb):KLu(WO$_4$)$_2$ nanoparticles with temperature in the range 22 – 250 ºC after excitation at 808 nm. (b) Energy level diagram and emission generated by upconversion after excitation at 808 nm for Ho^{3+}, Tm^{3+}, and Yb^{3+} in KLu(WO$_4$)$_2$ nanoparticles. (c) I$_{red}$/I$_{green}$ in the range of temperatures 22-50 ºC. (d) Temperature dependence of the relative sensitivity for the (Ho,Tm,Yb):KLu(WO$_4$)$_2$ nanoparticles.

3.2.(Er,Yb):NaY$_2$F$_5$O nanoparticles

The entity to which the temperature wants to be determined may be in movement, or in a environment where others parameters, such as pH and oxygen concentration, can affect the luminescent intensity of the emission lines of the nanoparticles. An alternative means of temperature sensing that overcomes these limitations is lifetime thermometry, although it has been scarcely used with up-converting materials [31,32]. An additional advantage of this technique for thermometry consists of the temperature estimation from the measurement of a single parameter (lifetime), therefore it is to a first approximation calibration-free. The use of systems that incorporate non-radiative relaxation and multiphonon phenomena, responsible for the shortening of fluorescence lifetime decays, such as oxides instead of fluorides, might allow considering this technique as an alternative to the more conventionally used fluorescence intensity ratio technique. (Er,Yb):NaY$_2$F$_5$O nanoparticles are promising candidates for this approach [31] since

their phononic response is extended to longer wavenumbers with respect to pure fluorides, (Er,Yb):NaYF$_4$ for instance, see the Raman spectra in Figure 3. This extended phononic response allows for a more easy activation of the non-radiative relaxation and multiphonon phenomena, similar to what is happening with oxides [33]. This is due to the fact that the smaller the number of phonons required to cover the energy gap between two levels, the higher the non-radiative multiphonon rate to depopulate an excited energy level to another one, as described by the phenomenological model of Riserberg and Moos [34]. Therefore, by increasing the phonon energy values in oxifluorides when compared to fluorides, induces the enhancement of the non-radiative processes, which shorten the experimental decay times.
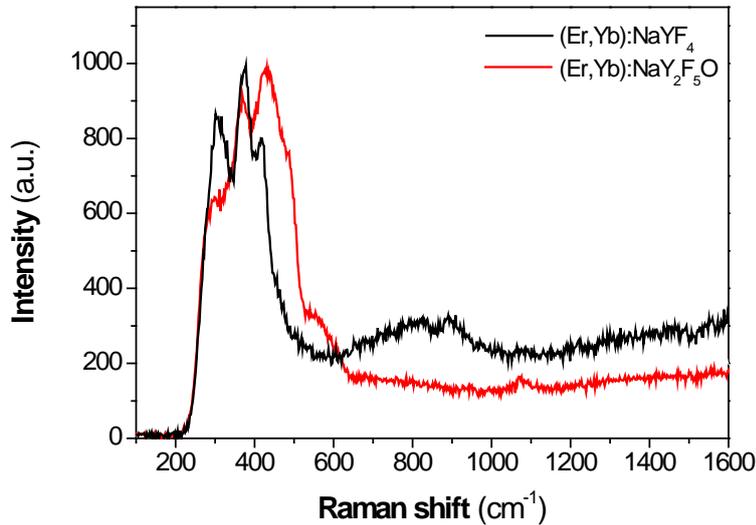
Figure 3. Raman spectra of (Er,Yb):NaYF$_4$ and (Er,Yb):NaY$_2$F$_5$O nanoparticles.

Figure 4(a) shows a TEM image of the (Er,Yb):NaY$_2$F$_5$O nanoparticles used in this work. They exhibit rod like morphologies, with diameters around 70-80 nm and lengths around 250 nm, as can be seen in the histograms provided in Figures 4 (b) and (c). However, these particles tend to be densely agglomerated. It is clear, thus, that for real applications, the morphological characteristics of the samples used in this work must be improved, but their quality is good enough to provide a trustable "proof of concept" of the potentiality of lifetime thermometry in the range of moderate temperatures.
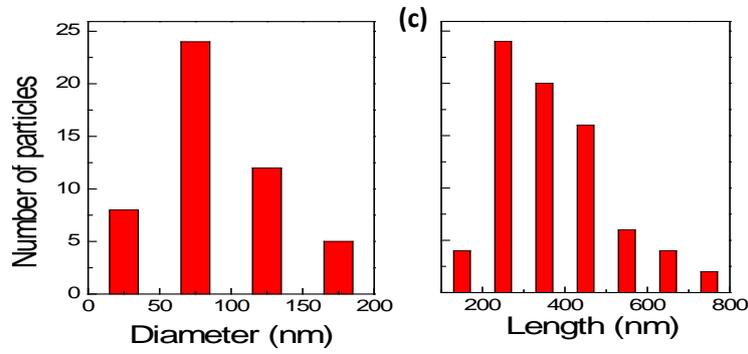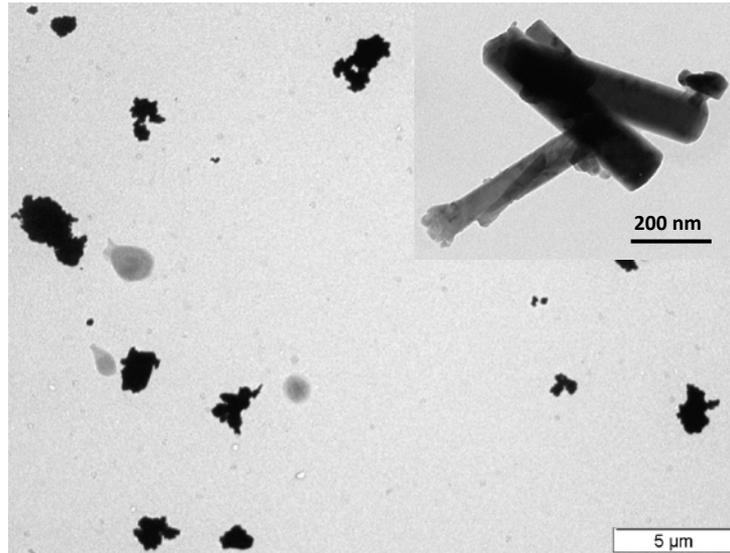
Figure 4. (a) TEM image of (Er,Yb):NaY$_2$F$_5$O nanoparticles. Histograms showing (b) the diameter and (c) lengths of the nanoparticles.

Figure 5(a) shows the emission spectrum of (Er,Yb):NaY$_2$F$_5$O nanoparticles after excitation at 980 nm. It consists mainly in two emission bands: a weak emission band in the green associated to the $^2H_{11/2}$, $^4S_{3/2} \rightarrow$ $^4I_{15/2}$ transitions of Er^{3+} and another more intense emission band in the red associated to the $^4F_{9/2} \rightarrow$ $^4I_{15/2}$ transition of Er^{3+}. The temperature dependent normalized lifetime, defined as $\tau_{nor}(T) = \tau(T) / \tau(RT)$, where $\tau(T)$ is the fluorescence lifetime measured at a temperature T, and $\tau(RT)$ is the fluorescence lifetime measured at room temperature, of the 545 nm and 660 nm emission lines in the range of RT to 60ºC are shown in Figure 5 (b). For that we analyzed only the decay part of the luminescent lifetimes, thus avoiding the rise time inherent in the energy transfer upconversion process, using the following expression: $\tau = \dfrac{\int I(t) \cdot t \cdot dt}{\int I(t) \cdot dt}$. In both cases we observed a linear decrease of the lifetime values when the temperature increased. However, the slope of the evolution of the lifetime associated with the 545 nm emission

line is higher, which will provide better temperature estimation sensitivity. In fact, the lifetime thermal coefficients (α_T), defined as the slope of the normalized lifetime vs. temperature, are 0.015 ºC^{-1} and 0.007 ºC^{-1}, thus we can consider that α_T (545 nm) ≈ 2 α_T (660 nm). This reduced thermal quenching value for the red emission is not surprising, since it has been previously reported for Er^{3+}-doped glasses in the range of temperatures between 10 K and room temperature [35]. It should be noted here that the high sensitivity observed for the green emission lays in the order of that previously obtained for other lanthanide doped systems [36-38] and quantum dots [39] pumped in the UV and blue regions of the electromagnetic spectrum, furthermore, it shows a better performance than gold nanoclusters pumped in the green [40].
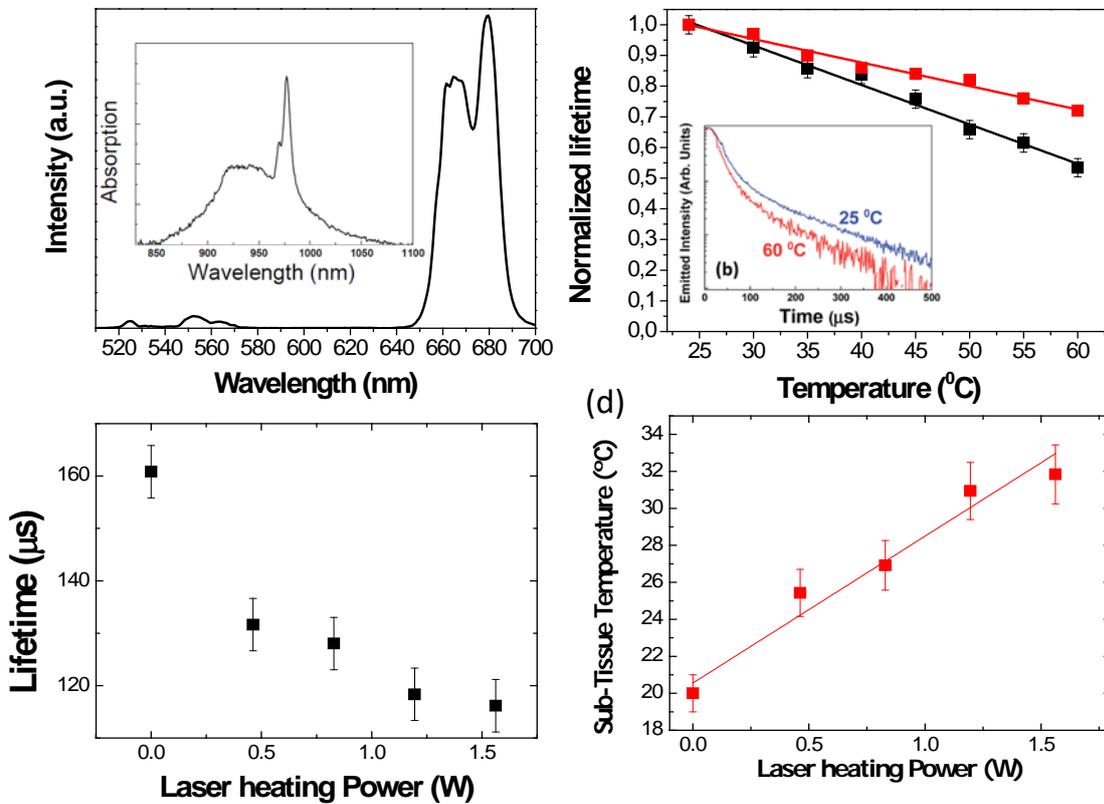
Figure 5. (a) Emission spectra of (Er,Yb):NaY$_2$F$_5$O nanoparticles after pumping at 980 nm. Inset shows the absorption spectrum of these nanoparticles in the 825-1100 nm region. (b) Normalized lifetime values as a function of temperature for the 545 nm and 660 nm emission lines. Inset shows the fluorescence decay curves of the 545 nm emission line at 25 and 60 ºC (c) Effect of the heating laser emitting at 1090 nm on the lifetime values of the 545 nm emission line on the nanoparticles introduced in chicken breast. (d) Ex-vivo temperature increment measured through lifetime variations in the 545 nm emission line of (Er,Yb):NaY$_2$F$_5$O nanoparticles as a function of the increase of the laser heating power.
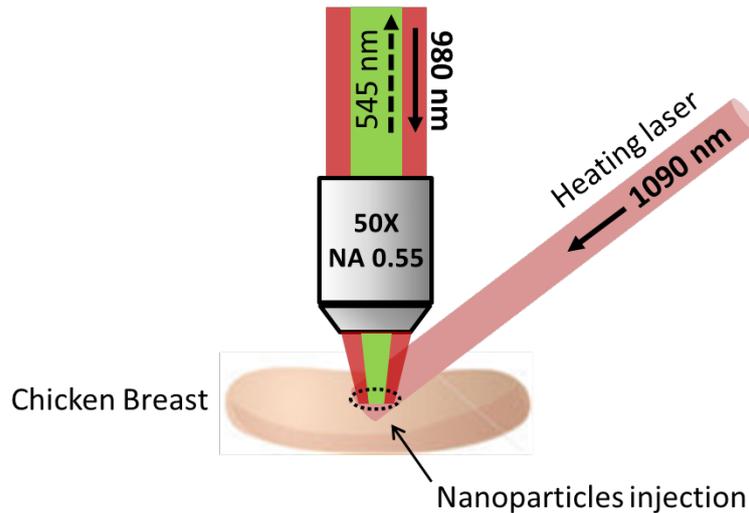
Figure 6. Scheme of the experimental set-up used in the ex-vivo thermal sensing experiment of sub-tissue temperature determination in chicken breast.

In order to show the potentiality of the (Er,Yb):NaY$_2$F$_5$O nanoparticles as a practical nano-thermometer for moderate temperatures, ex-vivo thermal sensing experiment of sub-tissue temperature determination in chicken breast were carried out as a function of the power of a heating laser emitting at 1090 nm. Figure 6 shows a scheme of the experimental set-up used. (Er,Yb):NaY$_2$F$_5$O were dispersed in water, and injected into a fresh chicken breast at a depth of 1 mm. A 1090 nm continuous laser beam was slightly focused into the injection's area and used as the heating beam due to the non-vanishing absorption coefficient of tissues at this wavelength (because of the presence of water). Optical excitation was achieved by using a 980 nm diode laser and the luminescence generated was first collected and collimated by using a low numerical aperture microscope objective and later it was focused into a photomultiplier by a using a single lens. Figure 5(c) shows the decrease of the lifetime of the 545 nm emission line when we increased the power of the heating laser focused inside the chicken breast. Since (Er,Yb):NaY$_2$F$_5$O nanoparticles do not absorb energy at 1090 nm (see inset in Figure 5(a)), the reduction of the lifetime is due to the heating of the chicken breast tissues induced by the laser. By combining these data with those of the calibration previously performed (see Figure 5(b)), we can determine the temperature inside the chicken breast, and we show it as a function of the laser heating power in Figure 5(d).

4. Conclusions

In conclusion, we have shown alternative luminescence thermometry techniques to the most commonly used fluorescence intensity ratio technique for moderate temperature sensing purposes. (Ho,Tm,Yb):KLu(WO$_4$)$_2$ nanoparticles can be used as an efficient luminescence temperature sensor using the temperature-dependent ratio of two emission lines. From another side, (Er,Yb):NaY$_2$F$_5$O nanoparticles show a great potentiality in moderate temperature sensing purposes using the lifetime thermometry technique, demonstrated by the ex-vivo sub-tissue temperature determination experiment in chicken breast.

References

[1] S. Wang, S. Westcott, W. Chen, J. Phys. Chem. B 106 (2002) 11203.

[2] L.D. Carlos

[3] G. Nenna, G. Flaminio, T. Fasolino, C. Miarini, R. Miscioscia, D. Palumbo, M. Pellegrino, Macromol. Symp. 247 (2007) 326.

[4] A. Ashkin, J.M. Dziedzic, T. Yamane, Nature 330 (1987) 769.

[5] H.B. Mao, T.L. Yang, P.S. Cremer, J. Am. Chem. Soc. 124 (2002) 4432.

[6] M. Jang, S.S. Kim, J. Lee, Exp. Mol. Med. 45 (2013) e45.

[7] D. Jaque, F. Vetrone, Nanoscale 4 (2012) 4301.

[8] C.D. Brites, P.P. Lima, N.J. Silva, A. Millan, V.S. Amaral, F. Palacio, L.D. Carlos, Nanoscale 4 (2012) 4799.

[9] S.W. Allison, G.T. Gillies, Rev. Sci. Instrum. 68 (1997) 2615.

[10] S. Uchiyama, Y. Matsumura, A. P. de Silva, K. Iwai, Anal. Chem. 75 (2003) 5926.

[11] A.L. Heyes, J. Lumin. 129 (2009) 2004.

[12] N.N. Dong, M. Pedroni, F. Piccinelli, G. Conti, A. Sbarbati, J.E. Ramirez-Hernandez, L.M. Maestro, M.C. Iglesias-de la Cruz, F. Capobianco, J.G. Sole, M. Bettinelli, D. Joque, and A. Speghini, ACS Nano 5 (2011) 8665.

[13] F. Vetrone, R. Naccache, A. Zamarron, A. Juarranz de la Fuente, F. Sanz-Rodriguez, L. M. Maestro, E. M. Rodriguez, D. Jaque, J.G. Sole, J.A. Capobianco, ACS Nano 4 (2010) 3254.

[14] L.H. Fischer, G.S. Harmns, O.S. Wolfbeis, Chem. Int. Ed. 50 (2011) 4546.

[15] V. Petrov, M.C. Pujol, X. Mateos, O. Silvestre, S. Rivier, M. Aguiló, R.M. Solé, J. Liu, U. Griebner, F. Díaz, Laser Photon. Rev. 1 (2007) 179.

[16] L.D. Deloach, S.A. Payne, L.L. Chase, L.K. Smith, W.L. Kway, W.F. Krupke, IEEE J. Quantum Electron. 29 (1993) 1179.

[17] M. Galceran, M. Pujol, M. C. Aguilo, M. Diaz, F. J. Sol-Gel Sci. Techn. 42 (2007) 79.

[18] V. Petrov, M.C. Pujol, X. Mateos, O. Silvestre, S. Rivier, M. Aguilo, R.M. Sole, J. Lin, U. Griebner, F. Diaz, Laser and Photon. Rev. 1 (2007) 179.

[19] V. Jambunathan, X. Mateos, M.C. Pujol, J.J. Carvajal, F. Diaz and M. Aguilo, J. Lumin. 131 (2011) 2212.

[20] R.H. Page, K.I. Schaffers, P.A. Waide, J.B. Tassano, S.A. Payne, W.F. Krupke, W.K. Bischel, J. Opt. Soc. Am. B 15 (1998) 996.

[21] E.W. Barrera, Lanthanide-based Dielectric Nanoparticles for Upconversion Luminescence, PhD Thesis, Universitat Rovira i Virgili, Tarragona, 2013.

[22] B. Dong, B. Cao, Y. He, Z. Liu, Z. Li, Z. Feng, Adv. Mater. 24 (2012) 1987.

[23] M.L. Debasu, D. Ananias, I. Pastoriza-Santos, L.M. Liz-Marzán, J. Rocha, L.D. Carlos, Adv. Mater. 25 (2013) 4868.

[24] L. Xing, Y. Xu, R. Wang, W. Xu, Z. Zhang, Opt. Lett. 39 (2014) 454.

[25] S.K. Singh, K. Kumar, S.B. Rai, Sens. Actuators A 149 (2009) 16.

[26] D. Li, Y. Wang, X. Zhang, K. Yang, L. Liu, Y. Song, Opt. Comm. 285 (2012) 1925.

[27] A. Pandey, V.K. Rai, Appl. Phys. B 113 (2013) 221.

[28] S.A. Wade, S.F. Collins, G.W. Baxter, J. Appl. Phys. 94 (2003) 4742.

[29] E.W. Barrera, M.C. Pujol, C. Cascales, J.J. Carvajal, X. Mateos, M. Aguilo, F. Diaz, Phys. Status Solidi C 8 (2011) 2676.

[30] B.S. Cao, Y.Y. He, Z.Q. Feng, Y. S. Li, B. Dong, Sensor Actuat. B 159 (2007) 8.

[31] Ol.A. Savchuk, P. Haro-Gonzalez, J.J. Carvajal, D. Jaque, J. Massons, M. Aguilo, F. Diaz, Nanoscale, 6 (2014) 9727.

[32] R.K. Benninger, Y. Koc, O. Hofmann, J. Requejo-Isidro, M.A. Neil, P.M. French, A.J. DeMello, Anal. Chem. 78 (2006) 2272.

[33] H.U. Güdel, M. Pollnau, J. Alloys Compd. 303-304 (2000) 307.

[34] L.A. Riseberg, H.W. Moss, Phys. Rev. 174 (1968) 429.

[35] S.K. Ghoshal, M.R. Sahar, M.S. Rohani, S. Sharma, Indian J. Pure Appl. Phys. 49 (2011) 509.

[36] K. Singh, K. Kumar, S.B. Rai, Sensors and Actuators A 149 (2009) 16.

[37] S.W. Allison, G.T. Gillies, A.J. Rondinone, M.R. Cates, Nanotechnology 14 (2003) 859.

[38] J. Yu, L. Sun, H. Peng and M.I.J. Stich, J. Mater. Chem. 20 (2010) 6975.

[39] Z.P. Cai, L. Xiao, H.Y. Xu, M. Mortier, J. Lumin. 129 (2009) 1994.

[40] P. Haro-González, L. Martínez-Maestro, I.R. Martín, J. García-Solé, D. Jaque, Small 8 (2012) 2652.